

Technical Paper

Non-Linear FEA of a Steel-Concrete Composite Deck under Increased Fatigue Loading and Damage Evaluation of the Concrete Elements by Stress Invariants

Daniel Apenyo*, Toshio Matsumura**, Takuji Kumano**, Hitoshi Wada***, Masashi Yamamoto*,
Chikako Fujiyama****

*MSc. of Eng., Japan Bridge Association (1-6-11 Nishi-Shinbashi, Minato-ku, Tokyo 105-0003)

**Dr. of Eng., Japan Bridge Association (1-6-11 Nishi-Shinbashi, Minato-ku, Tokyo 105-0003)

***BS. Civil Eng., Japan Bridge Association (1-6-11 Nishi-Shinbashi, Minato-ku, Tokyo 105-0003)

****Dr. of Eng., Associate Professor, Institute of Urban Innovation, Yokohama National University (79-5 Tokiwadai,
Hodogaya-ku, Yokohama-shi, 240-8501)

Strength and fatigue resistance of a Steel-concrete deck composite structure have been verified by wheel running tests however, fatigue damage process due to full-scale bridge loads isn't clear. The purpose of this research is to conduct a nonlinear finite element analysis on the composite structure under fatigue loading (8 times T-Load) and evaluate by stress invariants the damage in concrete elements. A cross section of elements beneath the wheel track between two adjacent ribs was evaluated using the Drucker-Prager criteria to confirm stress state of each element, identify critical elements and classify the damage pattern of a steel-concrete deck composite.

Keywords: Nonlinear Finite Element Analysis (FEA), Fatigue Analysis, Drucker-Prager Criteria, Steel-Concrete Composite Deck

1. BACKGROUND

Steel-concrete deck is a reinforced concrete slab with a steel plate at the bottom. This plate that works as tension reinforcement is connected to concrete by headed studs welded on the plate. Strength and fatigue resistance of the composite structure have already been verified by wheel running tests however, the fatigue damage process due to full scale bridge loading isn't clear.

Fatigue problems on both steel decks and reinforced concrete decks have been investigated both experimentally and analytically however, the number of investigations of steel-concrete composite decks is small¹⁾. In a study on the damage analysis of headed stud on the steel-concrete composite deck by numerical analysis, the failure process under fatigue loading considering a heavy load of 800KN (4 times T-Load) was conducted²⁾. The maximum mid-point deflection (8mm) obtained by fatigue analysis was 1.75 times larger than that obtained by static analysis. Also, in the fatigue analysis, this deflection did not increase with the increase in the number of loading cycles up to 100 million. However due to the bottom steel plate, damage inside the concrete remains invisible that makes it hard to obtain practical damage information. Therefore,

the purpose of this research is to conduct a nonlinear finite element analysis to a steel-concrete composite deck under increased fatigue loading of 1600KN (8 times T-Load) and evaluate by stress invariants the damage in the concrete elements.

1.1 Failure criteria and Stress Invariants

According to Hawkins and Mitchell³⁾, the failure mode of composite structures is greatly influenced by the mechanical properties of shear connectors. However, in formulating failure criteria for concrete materials under combined states of stress, agreement must be reached on a proper definition of failure. Criteria such as yielding, initiation of cracking, load-carrying capacity and extent of deformation have been used to define failure. A failure criterion of isotropic materials based upon state of stress must be an invariant function of state of stress that is independent of choice of coordinates system in which the stress is defined⁴⁾. This criterion can be applied to un-cracked concrete, however the cracked concrete is well known as a highly anisotropic material.

Considering a 3D element subjected to pressure loading, the components of stress tensor σ_{ij} are given in Figure 1. In the principal direction, the stress state at any point inside a concrete material can be defined by stress tensor σ_{ij} in terms of three

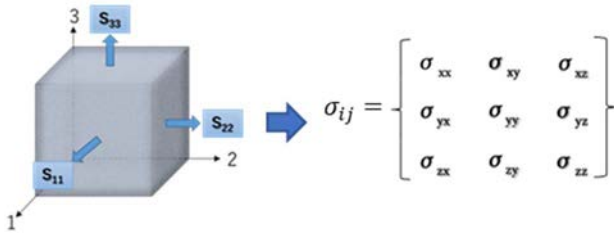


Fig. 1 Components of stress tensor in an element.

principal invariants I_1 , I_2 and I_3 . The stress tensor can also be decomposed into two components (Equation 1) i.e., a purely hydrostatic stress σ_m and a deviatoric stress S_{ij} part which represents state of pure shear. The invariants of stress deviator are expressed as J_1 , J_2 and J_3 .

$$\sigma_{ij} = S_{ij} + \sigma_m \delta_{ij} \quad (1)$$

1.2 Non-Linear Finite Element Analysis

The numerical software used in the study is COM3 based on the Maekawa Concrete Model in which fatigue damage of concrete is comprehensively enhanced by the embedded constitutive laws⁵⁾ to consider; a) decrease of stiffness and plasticity accumulation by continuous fracturing of concrete in compression, b) decrease of tension stiffness by bond fatigue and c) decrease of shear transfer normal to crack by continuous deterioration of rough crack surface.

2. METHODOLOGY

2.1 Target Bridge

The target bridge (Figure 2) is a twin girder highway bridge supporting a steel-concrete composite deck of width 6m and average span 49m. The 260mm thick concrete slab with embedded reinforcing bars is connected to 8mm thick bottom steel plate by headed studs of diameter 16mm and with reinforcing ribs.

2.2 Modeling and Material properties

The analysis considers a half cross section of target bridge (Figure 2), modelled 20m in length and boundary conditions set as in Figure 3. The girder is constrained at the lower flange ends as a simply supported beam. For the half model of the bridge considering symmetry, the nodes at the centerline are constrained in the direction perpendicular to the bridge axis. Material strengths for concrete (compression strength, $f_c = 30$ MPa and tension strength, $f_t = 2.22$ MPa) and steel (main girder, yield strength, $f_y = 345$ MPa, cross girder, bottom plate, studs and ribs, yield strength, $f_y = 245$ MPa and Reinforcement bar (SD345), yield strength, $f_y = 345$ MPa) were applied.

The interface between the different materials to represent adhesion and friction are reproduced by bond elements with parameters as show in Table 1.

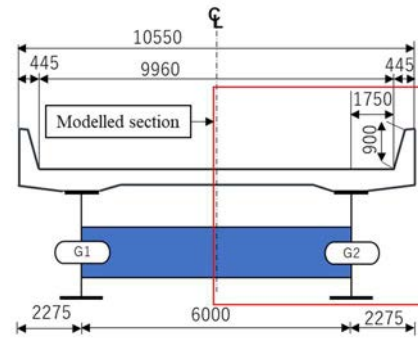


Fig. 2 Bridge cross section (dimension in mm).

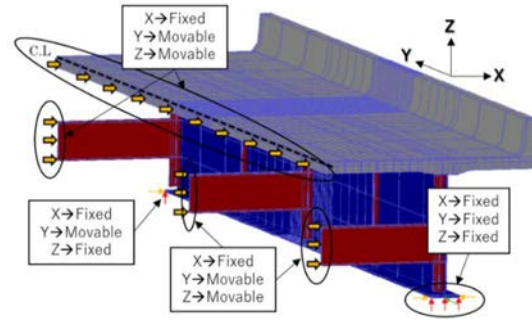


Fig. 3 Analysis model showing boundary conditions.

Table 1 Bond element properties

Parameter	Value
Shear stiffness in closure mode	76923 (N/mm ²)
Normal stiffness in closure mode	200000 (N/mm ²)
Normal/Shear stiffness in Open mode	15 (N/mm ²)
Initial Bond (Normal/Shear)	3 (N/mm ²)
Friction	0.5

Table 2 Fatigue loading cases

Analysis	Loading	Number of cycles
Case 1	800 KN (4 x T-Load)	10,000,000
Case 2	1600 KN (8 x T-Load)	1,000,000,000

2.3 Fatigue loading

The fatigue loading cases are shown in Table 2. T-Load is defined as a Truck Load specified by the Japanese Standard⁶⁾. In this study, excessive loads (not expected in reality on the actual bridge) are intentionally set to investigate failure process by nonlinear analysis. It is also assumed that the loads are symmetrically applied in the whole bridge model.

2.4 Bridge mid-point vertical displacement

The bridge mid-point vertical displacement was evaluated according to load cases in Table 2. According to Figure 4, Case 2 deflection history shows that the slab mid-point vertical displacement increased with increase in the number of cycles whereas in Case 1, the maximum displacement remained constant regardless. In the first loading cycle, Case 1 produced a maximum deflection of 7mm as compared to 16mm for Case 2

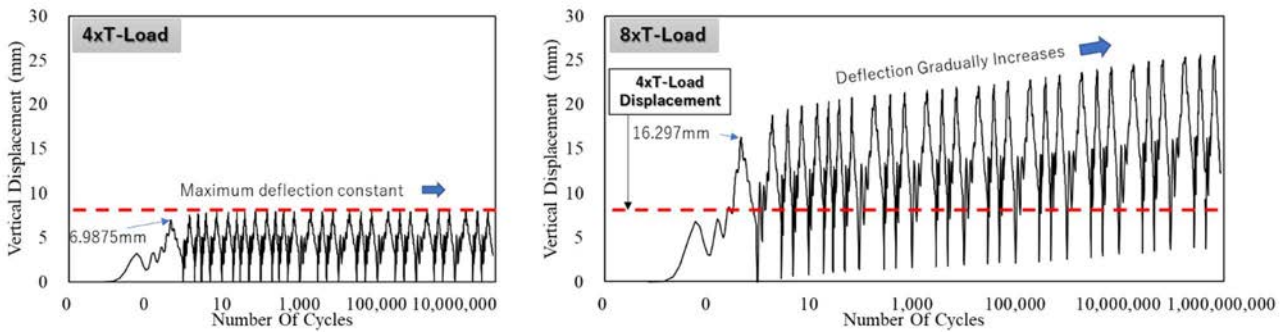


Fig. 4 Bridge mid-point displacement history.

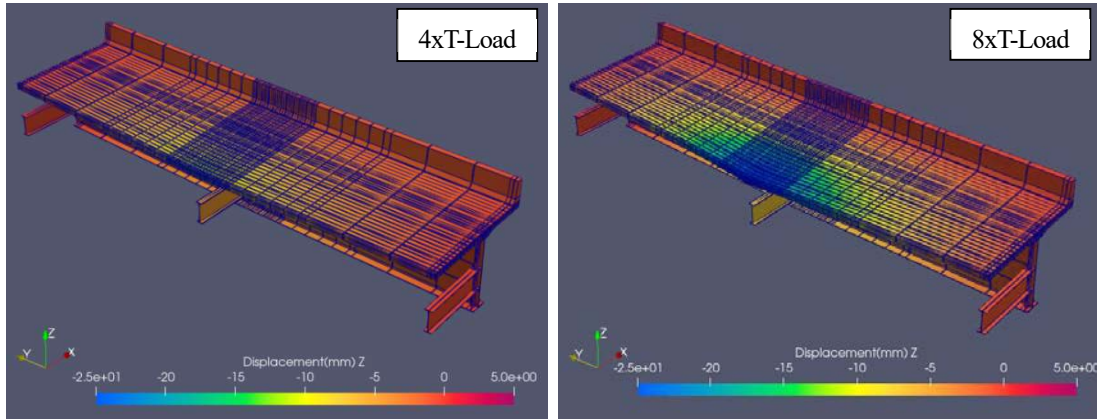


Fig. 5 Bridge deformed shape (scale factor = 50) with load at the center of slab (first cycle loading).

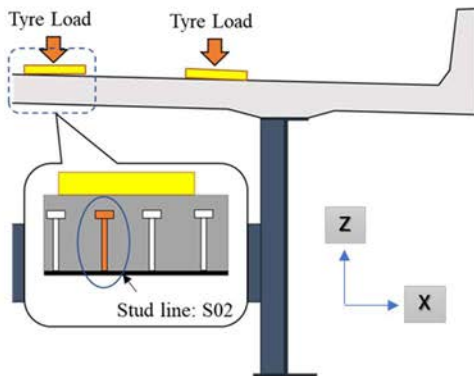


Fig. 6 Stud line S02 location.

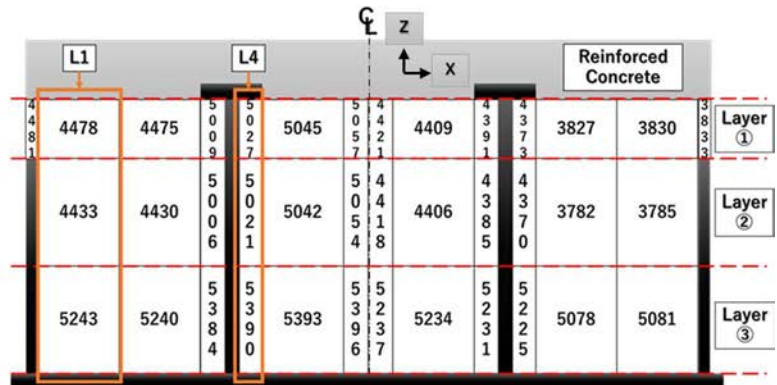


Fig. 7 Cross section showing focus elements at stud line S02.

attributed to difference in the loading conditions. Figure 5 shows bridge deformation (scale factor = 50) with load at center of slab.

3. ELEMENT DAMAGE EVALUATION

3.1 Focus area and Load consideration.

The area of focus is a cross section beneath the wheel track along stud line S02 as indicated in Figure 6. A detailed cross section of focus elements for each layer of concrete, located between adjacent ribs is shown in Figure 7. Additionally, damage evaluation of cross section based on element location i.e. near the rib (L1) and beneath the stud head (L4) have been considered as indicated in Figure 7.

According to the bridge mid-point displacement results in Section 2.4, only damage in concrete by load Case 2 (Table 2)

described in Section 2.3 was evaluated for invariant stress states.

3.2 Drucker-Prager yield criterion

The Drucker-Prager yield criterion is a pressure independent model often referred to as the smooth version of Mohr-Coulomb yield surface. This has been widely used in the geotechnical and concrete engineering field to determine whether a material has failed or undergone plastic yielding when subjected to loading, based on the first invariant stress (I_1) and the second invariant of the deviatoric part of stress ($\sqrt{J_2}$) relationship. The damage evaluation is derived from the Drucker-Prager failure boundary surface governed by equation 2 below.

$$\sqrt{J_2} = \alpha I_1 + \beta \quad (2)$$

$$I_1 = \sigma_{xx} + \sigma_{yy} + \sigma_{zz} \quad (2a)$$

$$\sqrt{J_2} = \sqrt{1/6 [(\sigma_{xx} - \sigma_{yy})^2 + (\sigma_{yy} - \sigma_{zz})^2 + (\sigma_{zz} - \sigma_{xx})^2] + (\tau_{xy}^2 + \tau_{yz}^2 + \tau_{zx}^2)} \quad (2b)$$

Where I_1 is the first invariant of Cauchy stress given by Equation 2a, J_2 is the second invariant of the deviatoric part of Cauchy stress derived from Equation 2b and α , β are parameters determined from experiments. Also the $I_1 - \sqrt{J_2}$ graph can be used to confirm element confinement (Figure 8).

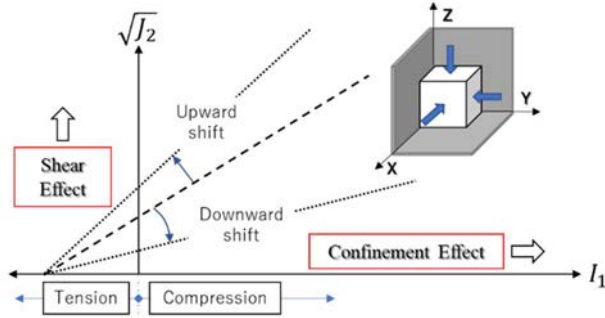


Fig. 8 Confinement indicator.

3.3 Tension and compression capacities of concrete

The first invariant of stress, I_1 is an indicator of both tension and compression in an element. Based on the tension strength, f_t and compression strength, f'_c of concrete i.e. 2.22 MPa and 30 MPa respectively, the stress states given by Equations 3 and 4 to identify elements under high stress values have been defined.

$$\text{For compression side, } \frac{I_1}{f'_c} > 1.0 \quad (3)$$

$$\text{For tension side, } \frac{I_1}{f'_c} < -0.074 \quad (4)$$

3.4 Capacity of Shear

The second invariant of the deviatoric stress, $\sqrt{J_2}$ represents shear effect. Based on the theory of shear transfer capacity along a crack plane under monotonic loading⁵⁾, the maximum shear, τ_{max} is given by Equation 5.

$$\tau_{max} = 3.83f'_c \frac{1}{3} \text{ (MPa)} \quad (5)$$

In this study, the authors defined shear capacity as Equation 6 in order to apply to the general Drucker-Prager criteria.

$$\frac{\sqrt{J_2}}{f'_c} = \frac{\tau_{max}}{f'_c} > 0.4 \quad (6)$$

4. RESULTS AND DISCUSSIONS

4.1 Failure mode classification

Figure 9 shows the $I_1 - \sqrt{J_2}$ relationship for selected elements (half of focus cross section) in each layer depicting the stress state at selected loading cycles (1, 10,000 and 1,000,000,000). However, an evaluation of all cross-section elements was conducted and failure modes explained in Section 3 were classified as shown in Figures 10-a, 10-b and 10-c.

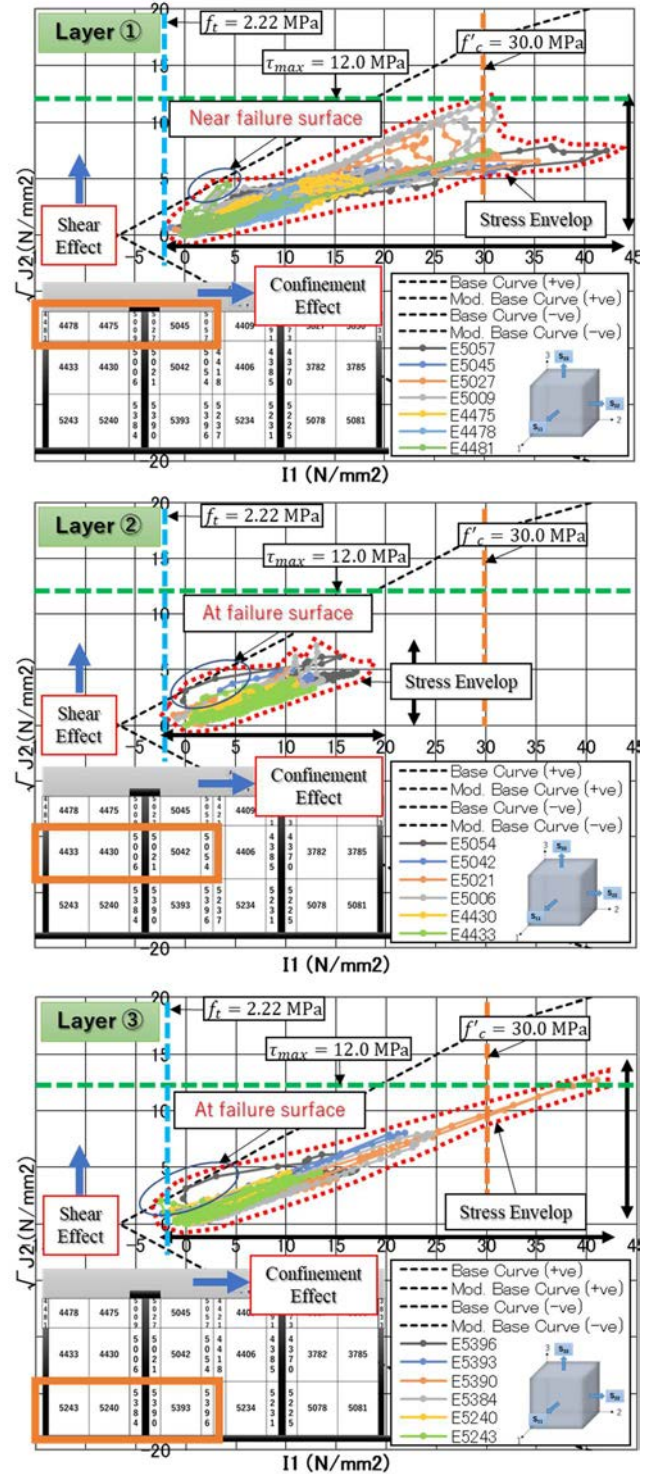


Fig. 9 Drucker-Prager relationship.

In Figure 10-a, high compression stresses exceeding 30 MPa occurred at the first layer on elements located directly above the rib, beneath the stud head, between the two studs and also in third layer near the bottom of the stud, attributed to the global deformation of the deck slab. Additionally, for regions beneath the stud head and at the bottom of stud, local deformation of both the stud and bottom steel plate causes confinement to the elements thus a high compression.

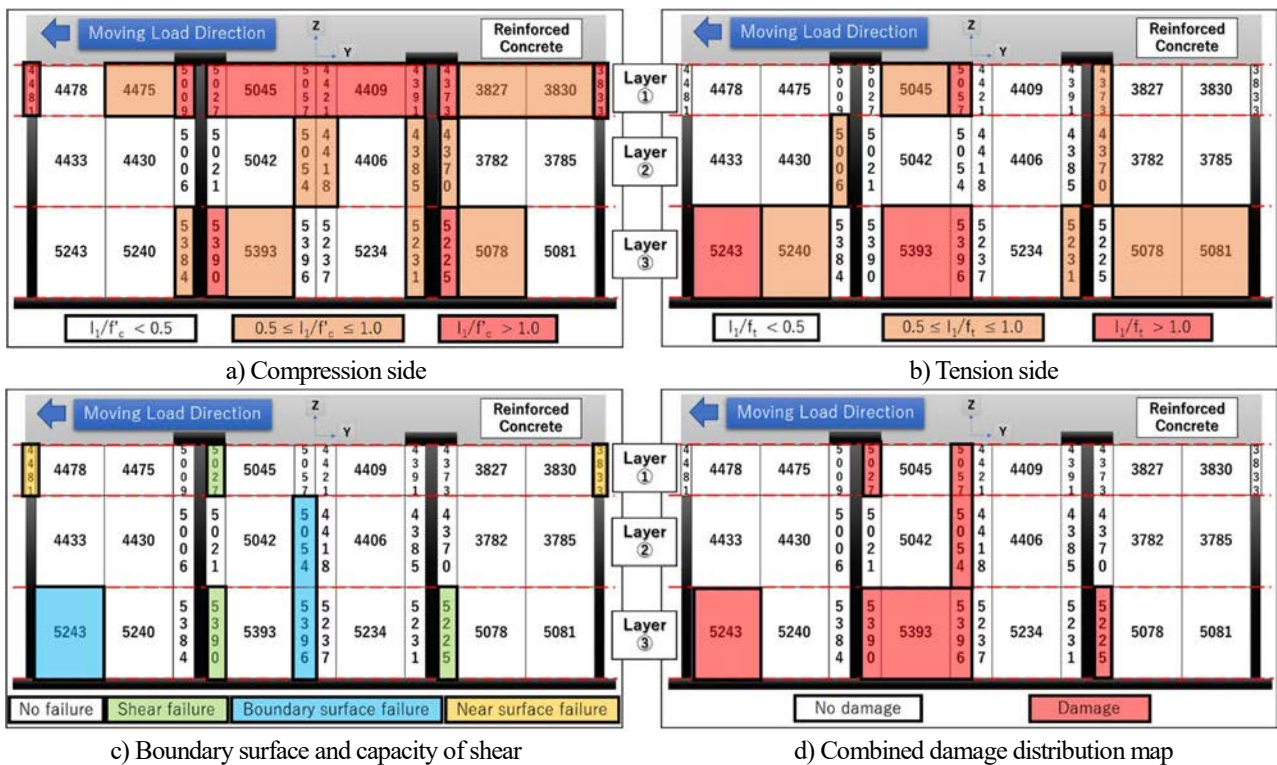


Fig 10 Element failure mode classification.

Figure 10-b, shows elements in tension failure attributed to global deformation of the deck slab. Generally, layer 1 element at center, layer 3 elements near the rib and element at slab center experienced high-tension stress exceeding 2.22 MPa.

Figure 10-c, shear failure occurs at elements in the region below the stud head and at the bottom of stud. In this region, as compressive stress increases due to element confinement, shear failure occurs. Failure considering the Drucker-Prager yield surface was confirmed at elements near bottom of the rib and at the centroid of the slab.

The combined damage distribution (Figure 10-d) shows that, elements in the forward direction of moving load are more susceptible to damage as compared to those on the opposite side.

4.2 Invariant stress envelope

The stress envelop in Figure 9 for the 3 layers and Table 3 shows the invariant stress range for each layer during the entire loading history. Layer 1 is characterized by an elongation on I_1 axis and wide distribution on the $\sqrt{J_2}$ axis with high compression stress values due to element confinement. Layer 2 has a shorter distribution implying low stress values due to proximity to neutral axis, while layer 3 has an elongated but thin distribution on both axes. In layer 3, the elongated distribution on the I_1 axis is due to element 5390 near bottom of the stud being subjected to high compressive stress due to confinement.

4.3 Comparison of elements stress state by location

Figure 11 shows the non-dimensional Drucker-Prager relationship comparing element stress state according to location,

Table 3 Invariant stress distribution.

	Layer 1	Layer 2	Layer 3
I_1 (MPa)	-1.0~42.2	-2.1~19.0	-3.3~42.4
$\sqrt{J_2}$ (MPa)	0~11.6	0~6.90	0~13.60

i.e. near the rib (L1) and beneath the stud (L4).

Near the rib (L1: Elements 4478 and 5243), all elements experience compressive stress less than 50% of 30 MPa due to minimal confinement effect. However, due to global deformation of slab, element 5243 located at the bottom exhibits failure on tension side as stress path is outside failure boundary surface and also the maximum tension stress exceeds 2.22 MPa.

Beneath the stud head (L4: Elements 5027 and 5390), all elements experience high compression due to the local bending behaviour of the stud and the global deformation of the bottom plate that causes element confinement. In element 5027, compression stress exceeds 30.0 MPa by about 18 % in the first loading cycle and further exceeds to about 49% as the loading cycle increases. After shear failure occurs, compressive stress decreases. Element 5390, compression stress only exceeds 30.0 MPa by 37% in the first loading cycle but reduces after shear failure has occurred.

5. CONCLUSION

The damage of concrete element due to fatigue loading (8 x T-Load) assessed by stress invariants showed that;

1. Most damaged elements are located in layer 3 while layer 1 elements experience high compression stresses in excess of 30 MPa. However, from the bridge centroid, the

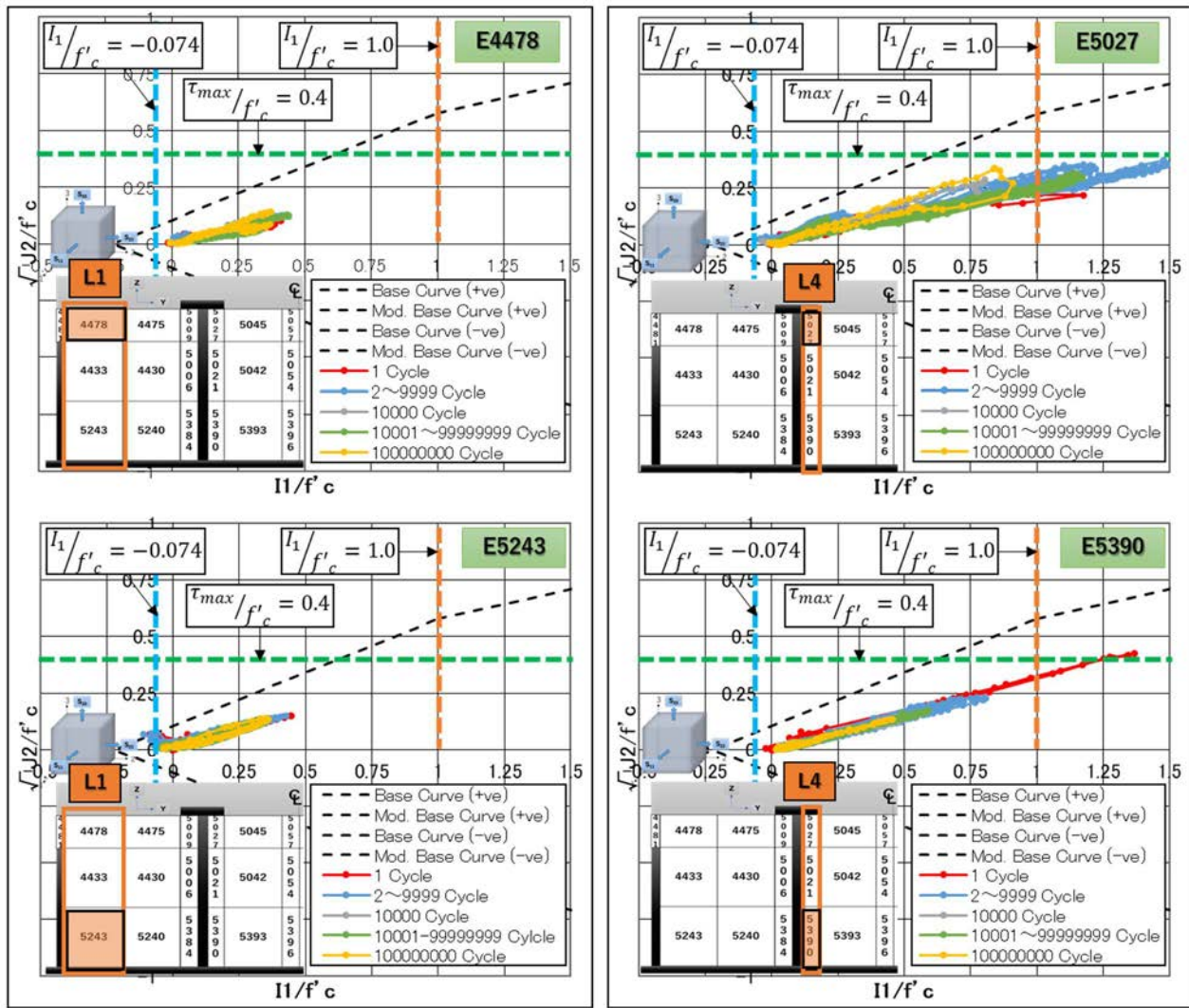


Fig. 11 Drucker-Prager relationship (non-dimensional) according to element locations L1 and L4.

damage distribution shows elements in the forward direction of moving load are more susceptible to damage as compared to elements on the opposite side.

2. At the rib, for element above, high compressive stress was observed while near the bottom, element failed in tension and failure confirmed by Drucker-Prager yield criterion.
3. Elements beneath the stud head and at bottom experienced high compressive stresses and shear failure was confirmed.
4. At the slab centroid, layer 1 is in high compression however, failure is governed by high tension stress at both layer 1 and 3 elements. Also, failure of elements in layer 2 and 3 were also confirmed by the Drucker-Prager criterion.

The results of this research based on stress invariants alone are inadequate to predict damage. Therefore, consideration for strain evaluation, stud deformation, etc. are recommended to fully comprehend damage in steel-concrete composite decks.

ACKNOWLEDGEMENT

We are grateful to Japan Bridge Association for the funding and Yokohama National University for the non-linear analytical tools and work environment for the research.

REFERENCES

- 1) C. Fujiyama and K. Maekawa: Fatigue Damage Assessment for Steel-Concrete Composite Deck, Society for Social Management Systems Internet Journal, 6(1), March 2010.
- 2) C. Fujiyama, H. Hoshina, H. Wada, T. Kumano and T. Matsumura: Fatigue Damage Analysis of Steel-concrete Composite Bridge deck by FEM, MECHCOMP3, International Conference on Mechanics of Composites, 2017, Italy.
- 3) M. N. Hawkins and D. Mitchell: Seismic response of composite shear connectors, Journal of Structural Engineering, 110(9), pp.2120-2136, 1984.
- 4) Wai-Fah Chen and Atef F. Saleeb: Constitutive Equations for Engineering Materials, Vol. 1, pp. 251-347, Elsevier, Netherlands, 1994.
- 5) K. Maekawa, A. Pimanmas and H. Okamura: Nonlinear Mechanics of Reinforce Concrete, pp. 125-175, Spon Press, London, 2003.
- 6) Japan Road Association: Specifications for highway bridges part 1, p. 94, 2017 (in Japanese).

(Received July 8, 2022)

(Accepted September 9, 2022)